

Improvements in Global Climate Model Microphysics Using a Consistent Representation of Ice Particle Properties

TRUDE EIDHAMMER AND HUGH MORRISON

National Center for Atmospheric Research, a Boulder, Colorado

DAVID MITCHELL

Division of Atmospheric Sciences, Desert Research Institute, Reno, Nevada

ANDREW GETTELMAN

National Center for Atmospheric Research, Boulder, Colorado

EHSAN ERFANI

Division of Atmospheric Sciences, Desert Research Institute, Reno, Nevada

(Manuscript received 6 January 2016, in final form 30 August 2016)

ABSTRACT

This paper describes a new approach for representing ice microphysics in climate models. In contrast with most previous schemes, this approach does not include separate categories for cloud and precipitating ice and instead uses a single two-moment category to represent all solid hydrometeors. Thus, there is no need for an ice “autoconversion” size threshold parameter, which has a critical impact on simulated climate in the Community Atmosphere Model (CAM5) yet is poorly constrained by theory or observations. Further, in the new treatment, all ice microphysical processes and parameters, including ice effective radius and mean fall speed, are formulated self-consistently and flexibly based on empirical ice particle mass-size and projected area-size relationships. This means that the scheme can represent the physical coupling between bulk particle density, mean fall speed, and effective radius, which is not possible in current schemes. Two different methods for specifying these relationships based on observations are proposed. The new scheme is tested in global simulations using CAM5. Differences in simulations using the two methods for specifying the mass- and projected area-size relationships, particularly the cloud radiative forcing, are attributable mainly to the effects on mean ice particle fall speed, impacting sedimentation and ice water path. With some tuning of parameters involved in calculating homogeneous freezing it produces a similar climate compared to the simulations using the original CAM5 microphysics. Thus, it can produce a comparable climate while improving the physical basis and self-consistency of ice particle properties and parameters.

1. Introduction

The parameterization of ice microphysics is an important component of climate modeling. In general circulation models (GCMs), it directly affects cloud radiative forcing by impacting the microphysical and optical properties of

ice-containing clouds (e.g., Gettelman et al. 2010). It also affects circulation through latent heating and cooling and the hydrologic cycle through precipitation formation, growth, and fallout. Ice microphysics has a critical impact on mixed-phase cloud properties by controlling the conversion of liquid water to ice (Gettelman et al. 2010; Lawson and Gettelman 2014). For example, changes in ice particle fall speed based on observed particle size distributions yielded large changes in cirrus coverage and ice water path, leading to decreases in the cloud radiative forcing up to 5 W m^{-2} in the tropics (Mitchell et al. 2008).

The representation of ice microphysics in atmospheric models, including GCMs, is highly uncertain. This is due

^aThe National Center for Atmospheric Research is sponsored by the National Science Foundation.

Corresponding author address: Trude Eidhammer, NCAR, P.O. Box 3000, Boulder, CO 80503.
E-mail: trude@ucar.edu

to uncertainty in basic knowledge of microphysical processes rates such as vapor diffusional growth and aggregation, as well as the inherent complexity of ice hydrometeors in the real atmosphere. To represent the range of ice particles and their physical properties, current microphysics schemes typically use various hydrometeor categories defined by prescribed physical characteristics (e.g., shape, bulk density, terminal fall speeds, and so forth) that broadly describe a given “typical” particle type (e.g., Fowler et al. 1996; Hong et al. 2004; Milbrandt and Yau 2005; Thompson et al. 2008; Morrison and Gettelman 2008; Morrison et al. 2009). The simplicity of this approach is attractive, but partitioning into a limited number of predefined categories with fixed characteristics is problematic. For example, it necessitates the conversion of particles between categories, which is inherently artificial and often done without a strong theoretical or empirical basis, and this conversion leads to discrete and often large changes in particle properties.

Simplified bulk microphysics schemes are generally used in GCMs because these models are unable to resolve small-scale motions that drive cloud processes and because there is a need for computational efficiency. Nonetheless, schemes in GCMs have advanced considerably over the last few decades. For instance, they now typically include separate prognostic variables for liquid and ice (e.g., Fowler et al. 1996; Lohmann and Roeckner 1996; Rotstayn et al. 2000; Morrison and Gettelman 2008). Several schemes also use a bulk two-moment approach prognosing mass and number mixing ratios for one or more hydrometeor categories (e.g., Ghan et al. 1997; Lohmann et al. 1999; Ming et al. 2007; Morrison and Gettelman 2008; Posselt and Lohmann 2008), in contrast with earlier schemes prognosing mass only (e.g., Rasch and Kristjansson 1998). Some schemes include separate prognostic variables for cloud and precipitation water (e.g., Fowler et al. 1996; Lopez 2002; Posselt and Lohmann 2008; Walters et al. 2014; Gettelman and Morrison 2015), as opposed to using a diagnostic approach for precipitation hydrometeors (e.g., Ghan and Easter 1992; Morrison and Gettelman 2008). Nonetheless, microphysics schemes in GCMs remain simpler compared to those used in higher-resolution cloud and mesoscale models. In particular, for the ice phase, the effects of rimed particles (graupel and hail) are neglected and typically only two ice categories are used: small, pristine ice (“cloud ice”) and larger, precipitating ice (“snow”) (e.g., Gettelman and Morrison 2015). Conversion of mass between the cloud ice and snow categories is often parameterized similarly to the conversion between cloud water and rain in warm bulk microphysics schemes, with “autoconversion” representing the generation of

new snow particles from smaller ice particles and “accretion” representing the growth of existing snow particles by aggregation of cloud ice. Accretion is formulated by assuming continuous collection with a gravitational collection kernel, neglecting the fall speed of cloud ice, while autoconversion is treated in an ad hoc way that varies among schemes. For example, Rasch and Kristjansson (1998) represent ice autoconversion by converting mass in the cloud ice category in excess of a threshold mass mixing ratio to snow. Morrison and Gettelman (2008) and Gettelman and Morrison (2015) represent ice autoconversion by converting the mass and number of cloud ice larger than a threshold size D_{cs} over a specified conversion time scale.

For ice microphysics, autoconversion does not represent any single physical process since small ice particles can grow to larger ones through a combination of vapor diffusion, aggregation, and riming. This is in contrast to liquid microphysics, for which autoconversion represents the growth of embryo raindrops by collision-coalescence of cloud droplets, and cloud droplets and rain have distinct growth modes (vapor diffusion for cloud droplets and collision-coalescence for rain). Another important distinction is that both cloud droplets and small raindrops are well approximated by liquid spheres, whereas the physical properties of cloud ice and snow (density, shape, and terminal fall speed) in schemes vary widely. This means there is a discrete, physically unrealistic transition in particle properties when cloud ice is converted to snow. Thus, the separation of cloud ice and snow as distinct categories and inclusion of autoconversion does not have a strong physical basis.

Previous studies have shown a large sensitivity of CAM5 simulations to D_{cs} , with large impacts on long-wave cloud radiative forcing in particular (Zhang et al. 2013; Eidhammer et al. 2014). Because of this sensitivity, D_{cs} has been used as a tuning parameter in CAM5. Unfortunately, it is not possible to directly constrain values of D_{cs} from observations. Moreover, Eidhammer et al. (2014) did not find any particular value of D_{cs} that led to substantially better overall results for the simulated particle size distributions compared to in situ microphysical observations. This highlights challenges in applying the traditional approach separating cloud ice and snow with mass conversion occurring by “autoconversion.”

Another deficiency in most current schemes is that ice particle mass-size, projected area-size, and fall speed-size relationships are not applied in a self-consistent way. For example, a mass-size relationship (related to bulk particle density) is used to calculate the size distribution parameters, but the fall speed is usually calculated from a simple fall speed-size relationship that

does not include information about density. Thus, in most schemes an increase in the mean particle density leads to a decrease in the mean size and hence a decrease in the mean fall speed, which is unphysical. Self-consistency of these relationships and quantities in models is desired because they are physically coupled in nature (Mitchell et al. 2011). For instance, since both effective radius and mass-weighted mean fall speed depend on particle mass divided by projected area, a change in these relationships should be reflected in both effective radius and mean fall speed.

An alternative approach that evolves particle properties freely and self-consistently, instead of separating ice into different predefined categories, was first proposed in the bin microphysics scheme of Hashino and Tripoli (2007). Morrison and Grabowski (2008) developed a bulk scheme that separately prognoses ice mass mixing ratios grown by riming and vapor deposition, to improve the treatment of transitions between unrimed snow, rimed snow, and graupel. Harrington et al. (2013a,b) developed a bulk scheme that predicts habit evolution by prognosing the crystal mean “a” and “c” axis lengths. Morrison and Milbrandt (2015) predicted several bulk ice particle properties as they evolve through all relevant growth modes (vapor diffusion, riming, and aggregation) for a single ice category, called the predicted particle properties (P3) scheme. These approaches obviate the need for an ad hoc autoconversion process.

The efforts described above represent a broader shift in the representation of ice microphysics by emphasizing the prediction of bulk particle properties rather than separation of ice into various predefined categories with fixed properties, with a focus on high-resolution cloud and mesoscale models. This general approach is also used as the basis for the current study, but our focus is on implementation in a traditional GCM, specifically CAM5, by modifying its current two-moment bulk scheme (Morrison and Gettelman 2008; Gettelman and Morrison 2015, hereafter MG2). In this work, the ice microphysics component of MG2 has been replaced with a new parameterization that combines cloud ice and snow into a single ice-phase category and prognoses the ice mass and number mixing ratios. The goal is to develop a simple bulk scheme addressing the deficiencies noted above in current schemes, including the need for autoconversion and a poorly constrained D_{cs} parameter in MG2, as well as inconsistencies in how the mass-size, projected area-size, and fall speed-size relationships are utilized. Although there are microphysics schemes in GCMs that use only one ice category [e.g., the scheme described in Wilson and Ballard (1999) used in the Met Office Unified Model], to our knowledge, this is the first scheme in a GCM to employ a single ice

category centered on the particle property approach (i.e., a physically based and self-consistent representation of the particle mass-size, projected area-size, and fall speed-size relationships for all relevant processes and parameters). The purpose of this paper is to document the new scheme and show “proof of concept” in its implementation and use in a GCM.

In the new scheme, observations are used to formulate relationships between particle mass, projected area, fall speed, and size that are used self-consistently for all relevant process rates and parameters. Consistent with the fact that large-scale models cannot resolve small-scale motion leading to the substantial production of rimed ice, combined with a need for simplicity and computational efficiency, the new scheme does not include the effects of riming on particle property evolution (note that the original MG2 scheme does not include these effects either). Two different methods for applying the mass-size and projected area-size relationships and process rate calculations are implemented and tested. This paper describes the new scheme and compares results with those using the original MG2 scheme and observations.

The remainder of the paper is organized as follows. Section 2 presents the new approach and a description of modifications to the MG2 scheme. Section 3 gives an overview of the model setup and observations used to compare with the model. Results are described in section 4. Finally, a summary and conclusions are presented in section 5.

2. Scheme description

The particle size distribution (PSD) for each hydrometeor category in MG2 (cloud droplets, cloud ice, rain, and snow) is represented by a three-parameter gamma function:

$$N'(D) = N_0 D^\mu e^{-\lambda D}, \quad (1)$$

where D is the maximum particle dimension, N_0 is the intercept parameter, μ is the shape parameter, and λ is the slope parameter. For solid hydrometeors, both the bulk number N and mass Q mixing ratios (units of kg^{-1} and kg kg^{-1} , respectively) for cloud ice and snow are prognosed and are related to the PSD in (1) by the following:

$$N = \int_0^{\infty} N_0 D^\mu e^{-\lambda D} dD, \quad \text{and} \quad (2)$$

$$Q = \int_0^{\infty} m(D) N_0 D^\mu e^{-\lambda D} dD. \quad (3)$$

Here m is the particle mass as a function of D . In many bulk schemes, including MG2, both cloud ice and snow particles are assumed to be spheres (e.g., Morrison and Gettelman 2008; Gettelman et al. 2010), and the mass is related to the spherical volume of the particles so that $m = \pi\rho_p D^3/6$ (where ρ_p is the bulk particle density).

To improve the realism of ice-phase microphysics in cloud and mesoscale models, some schemes (e.g., Thompson et al. 2008; Milbrandt et al. 2012) have moved away from parameterizing ice particles as spheres and instead represent nonspherical ice using power law mass-dimensional (m - D) relationships:

$$m = \alpha D^\beta, \quad (4)$$

where the parameters α and β are empirically determined constants that vary with different “types” of ice. However, using fixed m - D relationships for each ice category is still problematic. First, it leads to discrete and often large changes in the m - D relationship when there is conversion between ice categories, as noted in the introduction. Second, empirically derived constant values of α and β are valid over a limited size range of particles. For example, applying parameters for larger ice particles to smaller sizes (less than $\sim 100\text{ }\mu\text{m}$) can lead to a bulk density that is greater than that of solid ice, which is unphysical. Third, using constant m - D parameters cannot realistically capture particle growth histories (Sulia and Harrington 2011; Harrington et al. 2013a). The particle projected area-size (A - D) relationship is usually expressed in the same form as the m - D relationship:

$$A = \gamma D^\delta. \quad (5)$$

Using constant A - D parameters leads to similar problems as using constant m - D parameters.

The deficiencies mentioned above have led to the recent development of bulk schemes centered on the prediction of particle properties instead of assuming separate ice categories with fixed properties, allowing the m - D and A - D relationships (and other properties) to evolve smoothly (Hashino and Tripoli 2007; Morrison and Grabowski 2008; Harrington et al. 2013a,b; Morrison and Milbrandt 2015). The MG2 scheme is modified here to follow a similar approach. The main modifications are combining cloud ice and snow into a single ice-phase category and using particle m - D and A - D relationships consistently for all process and parameter calculations.

The three parameter gamma function for the PSD from MG2 is retained for the new single ice category approach. For the PSD shape, MG2 uses inverse exponential functions so that $\mu = 0$. In contrast, we improve

flexibility and allow nonzero μ in the modified scheme. Similar to Morrison and Grabowski (2008), here μ is from Heymsfield (2003) based on size distribution fits to observations of ice clouds:

$$\mu = 0.076\lambda^{0.8} - 2. \quad (6)$$

where λ has units of cm^{-1} . In the code μ is limited to a range from 0 to 6, corresponding to λ of 60 to 235 cm^{-1} . While Heymsfield (2003) showed negative μ for λ less than about 60 cm^{-1} , we constrain μ to be nonnegative so that $N'(D)$ is finite at $D = 0$. Two different methods are used to represent the m - D and A - D relationships, which affect parameters such as fall speed and effective radius as well as process rate calculations. The first method follows from the P3 scheme (Morrison and Milbrandt 2015), and the second follows from the approach proposed by Erfani and Mitchell (2016). Each method is described briefly below.

a. P3 method

The P3 scheme evolves the m - D and A - D relationships based upon the evolution of four prognostic ice variables: the ice mass, number, rime mass, and rime volume mixing ratios. These relationships evolve with the prognostic variables following a conceptual model of ice particle growth similar to Heymsfield (1982), including the effects of vapor deposition, aggregation, and riming. Since large-scale GCMs cannot resolve small-scale motion leading to the substantial production of rimed ice, the effects of riming and wet growth on particle properties are not included and only the prognostic ice mass and number mixing ratios (and temperature) are used to diagnose m - D and A - D in the current implementation.

For unrimed ice particles, P3 uses the empirical m - D relationship from Brown and Francis (1995) and A - D relationship from Mitchell et al. (1996), where $\gamma = 0.2285$ and $\delta = 1.88$ in cgs units. To avoid the aforementioned problem of extrapolating these relationships to small particle sizes, the m - D relationship is extended down to the size at which the particle mass is equal to that of a solid ice sphere with the same D . Particles smaller than this size are specified to have m - D and A - D relationships for spherical, solid ice. Since the m - D relationship varies across the size distribution using this approach, an inversion of incomplete gamma functions is needed to solve (3). Moreover, since the m - D and A - D (and hence fall speed- D) relationships vary for different regions of the size distribution, the bulk microphysical process rates and parameters integrated over the size distribution require the calculation of incomplete gamma functions. Given the computational expense of this, the bulk process rates

and parameters are precalculated and stored in a lookup table. Outputs from the lookup table are the mass and number weighted fall speeds, effective radius, and quantities related to the vapor deposition rate, ice self-collection rate, accretion rate of cloud water by ice, and accretion rate of rainwater by ice. In the model, these quantities are calculated using linear interpolation of the lookup table values as a function of N and Q , similar to the P3 approach. In the current implementation, values of N and Q in the lookup table for the calculations are given by $N = 8^k \times 10^{-10}$, and $Q = 5.1^k \times 10^{-16}$, where k is the set of integers from 1 to 20 (here N and Q have units of kg^{-1} and kg kg^{-1} , respectively). For accretion of rainwater by ice, there is an additional dimension added to the lookup table to account for the dependence on rain characteristics. This is done as a function of the rain mean volume diameter D_v , with lookup table values given by $D_v = 1.24^k \times 10^{-6}$ (D_v has units of m) and where k is the set of integers from 1 to 30.

An analysis of error from the P3 lookup table approach was done by calculating values for the quantities output from the lookup table, but using a much finer spacing for Q and N (96 points each for Q and N , compared to 20 each for the standard lookup table). Output quantities calculated by interpolation using the standard lookup table, following how the P3 approach is implemented in CAM5, were then directly compared to the finer mesh calculations. As an example, for the mass-weighted mean fall speed the mean relative error considering the entire range of Q and N is 9.4%, with 76.3% of points having <10% relative error. The mean absolute error (standard error) is 2.2 cm s^{-1} and is fairly constant for all values of mass-weighted mean fall speed. Thus, the largest relative errors occur when the fall speeds are very small (<10 cm s^{-1}). The mean bias is 0.6 cm s^{-1} . Mean relative or absolute error has little meaning for output quantities that vary by several orders of magnitude across the range of Q and N , such as the output related to ice self-collection. Thus, to assess accuracy we calculated a log-mean relative error. Considering all points except the ~10% that have zero error (since the logarithm is undefined in this instance), the log-mean relative error for the ice self-collection quantity is 12.3%, again dominated by error when the quantity itself is small. Finally, we note that recent work has further improved the P3 lookup table approach by using normalized ice size distributions, so that the lookup table is a function of Q/N rather than Q and N separately. This reduces the dimensionality of the lookup table by one, allowing for reduced error for a similar lookup table size. This approach may be used in future versions of the P3 approach implemented into CAM5.

b. Erfani and Mitchell (2016) approach

Erfani and Mitchell (2016) developed a second-order polynomial fit for the m - D relationship from observations, which covers a wide range of sizes. This fit has the following form:

$$\ln m = a_0 + a_1 \ln D + a_2 (\ln D)^2, \quad (7)$$

where a_0 , a_1 , and a_2 are constants determined from ground-based measurements of individual ice particle shape, m and D , and from observations of cloud ice particles from the small particles in cirrus (SPARTICUS) field campaign. The fit parameters are dependent on temperature and with separate parameter fits for “anvil” and “in situ”¹ cirrus. Parameter values are given in Table 1 of Erfani and Mitchell (2016). For the simulations presented herein, we use the parameters for in situ cirrus unless otherwise indicated. Erfani and Mitchell (2016) also developed a polynomial fit for the A - D relationship:

$$\ln A = b_0 + b_1 \ln D + b_2 (\ln D)^2 \quad (8)$$

with the constants b_0 , b_1 , and b_2 given in Table 2 of Erfani and Mitchell (2016).

Based on Erfani and Mitchell (2016), the polynomial fits can be reduced to simple power laws [e.g., Eqs. (4) and (5)] for sizes of interest, defined as the size most dominant for a given process or parameter (e.g., the PSD moments employed). Thus, each moment has different values for α and β , which can be determined from the polynomial fits by combining (4) and (7) and differentiating with respect to $\ln D$ to give (Erfani and Mitchell 2016)

$$\frac{d(\ln m)}{d(\ln D)} = \beta = a_1 + 2a_2 \ln D, \quad (9)$$

and α is found by combining (4) and (7) and rearranging terms, giving

$$\alpha = \frac{e^{a_0 + a_1 \ln D + a_2 (\ln D)^2}}{D^\beta}. \quad (10)$$

The A - D parameters γ and δ in (5) can be determined in the same manner:

$$\frac{d(\ln A)}{d(\ln D)} = \delta = b_1 + 2b_2 \ln D, \quad (11)$$

¹“In situ” refers to any cirrus that is not clearly linked to outflow from deep convection.

and

$$\gamma = \frac{e^{b_0 + b_1 \ln D + b_2 (\ln D)^2}}{D^\delta}. \quad (12)$$

The parameters α , β , γ , and δ , are calculated iteratively for each microphysical process from (9)–(12) using a representative particle size for that process, explained as follows. For sedimentation of ice mass (mass-weighted fall speed), the mass-weighted median dimension is used:

$$D_m = \frac{\beta + \mu + 0.67}{\lambda}, \quad (13)$$

For the sedimentation of ice number mixing ratio (number-weighted fall speed), median number-weighted dimension is used:

$$D_N = \frac{\mu + 0.67}{\lambda}. \quad (14)$$

The m - D and A - D parameters for calculating the collection of rain, cloud droplets, and self-collection of ice/snow and effective radius use the projected area-weighted median dimension:

$$D_A = \frac{\delta + \mu + 0.67}{\lambda}. \quad (15)$$

Finally, vapor depositional growth is mainly dependent on the first moment of the size distribution, and the size used is the first moment-weighted median dimension:

$$D_{m1} = \frac{1 + \mu + 0.67}{\lambda}. \quad (16)$$

The median dimension of interest above (D_x , where x represents m , A , N , or $m1$) are dependent on the unknown β (or δ), μ , and λ . The slope parameter λ is determined by the ratio of the mass and number mixing ratios by solving (2) and (3) and rearranging terms:

$$\lambda = \left[\frac{\alpha \Gamma(\beta + \mu + 1) N}{\Gamma(\mu + 1) Q} \right]^{1/\beta}. \quad (17)$$

Equations (6) and (9)–(17) are solved numerically by iteration for a given N , Q , and temperature with specification of the a_0 , a_1 , a_2 , b_0 , b_1 , and b_2 parameters from the fitted m - D and A - D relationships.

[Erfani and Mitchell \(2016\)](#) discuss errors in various quantities from assuming constant α , β , γ , and δ evaluated at a single characteristic D instead of using size-varying parameters. The errors are shown therein as a function of number-weighted mean particle

dimension, $\bar{D} = (\mu + 1)/\lambda$, for the effective diameter (Fig. 13 in [Erfani and Mitchell 2016](#)) and mass-weighted mean fall speed (Fig. 14 in [Erfani and Mitchell 2016](#)). For the mass-weighted fall speed, in our approach the α , β , γ , and δ parameters are calculated at a size corresponding to the mass-weighted median dimension D_m given by (13). The term \bar{D} can be expressed analytically in terms of D_m by $\bar{D}/D_m = (\mu + 1)/(\beta + \mu + 0.67)$. For $D_m = 500 \mu\text{m}$, corresponding to the calculations in [Erfani and Mitchell \(2016\)](#), for $\beta \sim 2$ this gives \bar{D} of $185 \mu\text{m}$ for $\mu = 0$ and $400 \mu\text{m}$ for $\mu = 6$ (the range of μ allowed in the scheme). As seen in Fig. 14 in [Erfani and Mitchell \(2016\)](#), errors in the mass-weighted fall speed are negligible for \bar{D} of $185 \mu\text{m}$ and larger but still small ($\sim 9\%$) for \bar{D} of $400 \mu\text{m}$. Similarly, for effective diameter the characteristic size is the projected area-weighted median dimension D_A given by (15). For $D_A = 500 \mu\text{m}$, again corresponding with the calculations in [Erfani and Mitchell \(2016\)](#), for $\delta \sim 2$ this gives the same values of \bar{D} as above. As seen in Fig. 13 in [Erfani and Mitchell \(2016\)](#), errors are negligible for \bar{D} of $185 \mu\text{m}$ and small ($\sim 6\%$) for \bar{D} of $400 \mu\text{m}$. Thus, overall errors are small using α , β , γ , and δ at a characteristic size.

The bulk process rates and parameters are precalculated and stored in a lookup table for consistency with the P3 approach. In addition to the dependencies on N , Q , and D_v , the lookup table for the [Erfani and Mitchell \(2016\)](#) approach includes an extra dimension to capture variation of the m - D and A - D parameters on temperature T . For creating the lookup table, the same values of N , Q , and D_v are used as in the P3 approach, while values of -60 , -47.5 , and -30°C are used for T .

c. Terminal fall speed and effective radius

Several processes involve the terminal fall speed of ice, such as sedimentation, collection of rain and cloud drops, and self-collection. Most microphysics schemes use a power-law relationship for the ice particle fall speed:

$$V = aD^b, \quad (18)$$

where a and b are determined empirically for different ice categories. An important problem with this approach is that the fall speed is not directly coupled to particle density, even though density is used elsewhere in the code. Thus, changes in particle density can lead to unphysical effects and inconsistencies as discussed in the introduction.

To address the shortcomings of using (18), we instead calculate fall speed as a function of D from the approach of [Mitchell and Heymsfield \(2005\)](#). We use Eqs. (6), (7), (8), (10), (11), and (12) therein, along with the parameter

values in that paper, with the exception that the turbulent correction term for aggregates is neglected [Heymansfield and Westbrook (2010) showed considerable error including this term for denser, more rimed particles]. In this approach, fall speed is calculated from the particle Reynolds and Best numbers, which are related to m - D and A - D (essentially, the fall speed depends on the ratio of particle mass and projected area). By using α , β , γ , and δ , the terminal fall speed is self-consistent with other processes that also depend on the m - D and A - D relationships. Unlike traditional schemes using (18), this approach gives the correct physical dependence of fall speed on particle density (via the m - D relationship) so that fall speed increases with increasing density, all else being equal. We note that for this approach, the empirical m - D and A - D relationships must be chosen with care to avoid large uncertainties in fall speed from using m - D and A - D relationships inconsistent with one another. Finally, the mean mass-weighted fall speed is found by multiplying the fall speed and particle mass as functions of D , numerically integrating the resulting expression over the size distribution, and then dividing by the total bulk mass. Similarly, the mean number-weighted fall speed is found by numerically integrating the fall speed over the size distribution and dividing by total bulk number.

Unlike terminal fall speed, most traditional schemes including MG2 have a dependence of ice effective radius on the m - D and A - D relationships, either explicitly or implicitly. However, in MG2 the ice effective radius is calculated using m - D and A - D relationships for spheres, which is inconsistent with the power-law parameterization of terminal fall speed in (18) with coefficients valid for nonspherical particles. In the modified scheme the ice effective radius (which is used by the radiation scheme) is also formulated from the m - D and A - D relationships [Morrison and Grabowski 2008, their Eq. (20)], but this is now consistent with the m - D and A - D relationships used for calculation of the fall speed and other microphysical processes. Thus, the modified scheme is able to represent the physical coupling between particle mass, projected area, fall speed, and effective radius discussed by Mitchell et al. (2011).

d. Microphysical process rate calculations

The modified scheme includes several ice microphysical processes similar to traditional bulk schemes, including nucleation, vapor deposition, sublimation, collection of cloud water and rain self-collection, and melting (assumed instantaneous at $+2^{\circ}\text{C}$ following MG2).

Ice nucleation is described in detail in Gettelman et al. (2010) and includes heterogeneous immersion freezing of dust competing with homogeneous freezing of sulfate

aerosols at temperatures $< -37^{\circ}\text{C}$ (Liu et al. 2007; Liu and Penner 2005). Deposition freezing is accounted for in mixed-phased clouds, following Meyers et al. (1992) with a constant nucleation rate for temperatures $< -20^{\circ}\text{C}$.

For vapor deposition and sublimation, the formulation as a function of D is given by Pruppacher and Klett [1997, their Eq. (13-76)], multiplied by the ventilation coefficients from Hall and Pruppacher (1976) [see Pruppacher and Klett 1997, their Eq. (13-89)]. The bulk deposition/sublimation rate is found by numerically integrating the resulting expression over the size distribution, using the lookup table approach outlined in section 2a.

Collection of cloud water by ice is described by continuous collection [e.g., Pruppacher and Klett 1997, their Eqs. (15-1) and (15-2)]. It is assumed that the fall speed and size of ice is much larger than that of the cloud droplets, so that the effects of droplet size and fall speed on the gravitational collection kernel are neglected, while the projected area and fall speed of ice are included. The collection efficiency depends on both ice and cloud water particle size, and the calculation is based on Stokes's law following Thompson et al. (2004). The bulk rate of ice growth from collection of cloud water is calculated by numerically integrating the growth rate of ice of a given D over the size distribution, again using the lookup table approach. Collection of rain by ice (and ice by falling rain) is calculated using the same method except that the area and fall speed of rain is included in the collection kernel, and the collection efficiency is specified to be 1. Self-aggregation of ice is calculated similarly to collection or rain by ice, including the effects of projected area and fall speed of ice. The efficiency of ice–ice collection is specified to be 0.5.

More details for these processes calculations are found in Morrison and Grabowski (2008) and Morrison and Milbrandt (2015) and are not repeated here for brevity. The process rate formulations themselves are the same using either the Erfani and Mitchell (2016) or P3 approaches for specifying the m - D and A - D relationships. Since the modified scheme includes only a single ice-phase category, conversion processes between categories in traditional schemes including MG2 are not needed. Thus, the modified scheme does not require specification and tuning of the uncertain autoconversion size threshold parameter D_{cs} , unlike MG2.

3. Model setup and observations

We use the atmospheric component (CAM) of the National Center for Atmospheric Research (NCAR) Community Earth System Model (CESM), version 5.3 (CAM5). This is the same model as used in Gettelman

et al. (2015) and essentially the same as the CAM5.0 model described by Neale et al. (2012). Simulations use the default MG2 scheme (Gettelman and Morrison 2015; Gettelman et al. 2015) or the modified version described in section 2 using either the P3 or Erfani and Mitchell (2016) approach to evolve the m - D and A - D relationships. Additional sensitivity tests with changes to parameters, using the Erfani and Mitchell (2016) approach are also described.

For this study, CAM5 was run for 6 years (from 2001 through 2006), with the first year as spinup. We used the Atmospheric Model Intercomparison Project (AMIP)-style configuration, with climatological monthly mean sea surface temperatures (SSTs) representing the period 1980–2000, repeated annually, and fixed CO₂ concentrations from year 2000. Aerosol emissions use estimates from year 2000. The horizontal resolution was $1.9^\circ \times 2.5^\circ$ with 30 vertical layers and an 1800-s time step for the model physics, with the finite-volume dynamical core. Global results were output as monthly means. We also output instantaneous microphysical parameters and state variables every 3 h over grid boxes overlapping the areas from two field campaigns that are used for model comparison. This setup for the output is the same as in Eidhammer et al. (2014) and is detailed in that paper.

Global results are compared among model simulations as well with shortwave and longwave cloud radiative forcing (SWCF and LWCF, respectively) estimates from the NASA Clouds and the Earth's Radiant Energy System (CERES) observations (Wielicki et al. 1996). We used the CERES EBAF 2.6 version, which contains data from *Terra* and *Aqua*. Uncertainties of the shortwave and longwave cloud radiative forcing are approximately 15% and are mainly from calibration and the determination of clear sky values (Gettelman et al. 2015). Ice water content is retrieved from *CloudSat* version 5.1 (Waliser et al. 2009) and Microwave Limb Sounder (MLS) version 2.2 (Wu et al. 2009) observations, similar to Gettelman et al. (2010). *CloudSat* is an active 94-GHz cloud radar with a horizontal footprint of 1.3 km cross track, 1.7 km along track, and 240-m vertical range. MLS is a microwave limb-viewing instrument with 200 km along track, 7 km cross track, and 4-km vertical resolution. There are large uncertainties in the retrieval of IWC from satellites (see discussion in Waliser et al. 2009).

Our results are also compared with microphysical observations from two field campaigns. These are the tropical composition, cloud and climate coupling (TC4) (Toon et al. 2010) mission in 2007 and the Atmospheric Radiation Measurements (ARM) spring cloud intensive operational period (IOP) in 2000 (ARM-IOP; Dong et al. 2002). These two campaigns and the observational datasets from them are the same as used in Eidhammer

et al. (2014), and more details about the observations and the comparison methodology between model and observations are described in that paper.

4. Results

The three main tests based on 6-yr global simulations are 1) original MG2, 2) the modified scheme with m - D and A - D relationships from Erfani and Mitchell (2016) (EM16), and 3) the modified scheme with m - D and A - D relationships from P3 (referred to as P3). Note that the EM16 and P3 use the same base CAM5 setup; the only difference is the lookup table that is used. Additional simulations were performed using EM16 with some modification of parameters related to homogeneous freezing of deliquescent aerosols to explore tuning of the cloud radiative forcing (EM16T1 and EM16T2). A simulation was also performed using EM16 but with m - D and A - D relationships derived from measurements in anvil instead of in situ cirrus. However, this simulation produces climate results very similar to the simulation with parameters for in situ cirrus (not shown). In all of the simulations with the modified scheme, the maximum ice number concentration is limited to 500 L^{-1} in order to limit large radiative forcing from high ice crystal number concentration (see section 4c). Furthermore, to account for the fact that the single ice category includes both small and large ice (snow), the size of detrained ice from deep convection and the size of homogeneously frozen cloud droplets are assumed to be $50 \mu\text{m}$ in radius instead of the default $25 \mu\text{m}$ in MG2. However, we note that tests modifying the size of detrained ice did not show large sensitivity in the climate results, such as LWCF and SWCF (not shown).

Mean state climate is quantified by globally averaged quantities for all of the main simulations (Table 1). Overall results are similar among the simulations. Common biases relative to observations (CERES) include large magnitudes of the SWCF, mainly in the tropics (up to -10 W m^{-2}), which is partly due to the parameterization of radiatively active cloud water within convective clouds (Gettelman et al. 2015). Biases in the global-mean LWCF are either positive or negative depending upon the simulation, with competing biases in the tropics and the midlatitudes. There are some notable differences among the simulations, including somewhat greater SWCF and LWCF in P3 and EM16 compared to MG2, discussed further below.

a. Cloud radiative forcing, ice water content, and effective radius

To investigate cloud radiative effects in the simulations further we analyze zonal means averaged over the

TABLE 1. Global mean statistics from the main simulations: radiative balance at the top of atmosphere R_{TOA} (W m^{-2}), SWCF (W m^{-2}) and LWCF (W m^{-2}) cloud forcing, LWP (g m^{-2}), IWP (g m^{-2}), high (above 400 hPa) cloud fraction (CF; %), and precipitation (PREC; mm day^{-1}) vs Global Precipitation Climate Project (GPCP). Observed LWCF and SWCF are from NASA's CERES observations. Note that IWP includes cloud ice and snow for MG2, with the contribution from cloud ice shown in parentheses.

	R_{TOA}	SWCF	LWCF	LWP	IWP	CF	PREC
MG2	2.50	-52.5	25.0	40.4	64.1 (14.2)	42.0	2.95
P3	0.56	-54.5	26.0	41.1	56.6	41.2	2.92
EM16	0.54	-58.9	30.4	41.4	63.5	44.8	2.82
EM16T1	0.95	-55.5	27.4	40.7	62.1	43.8	2.88
EM16T2	1.18	-53.4	25.6	40.1	60.1	43.3	2.92
Obs	—	-48.5	27.2	—	—	—	2.67
Uncertainty (%)	—	15%	15%	—	—	—	20%

5-yr period from 2002 through 2006. Figure 1 shows the SWCF and LWCF using MG2, EM16, and P3, as well as estimates from CERES observations. For EM16 and P3, the LWCF and SWCF are similar to those from MG2 in the midlatitudes. The largest differences between MG2 and simulations with the modified scheme are seen in the tropics, with EM16 and P3 producing larger SWCF and LWCF. This increase in the magnitude of the cloud forcing relative to MG2 is greatest over the west Pacific Ocean, over the Southeast Asia region, and over the Gulf of Mexico (Fig. 2), while over the southern continents the differences are smaller and opposite in sign. Overall, cloud radiative forcing from P3 is more similar to MG2 and is generally within a few W m^{-2} in the zonal mean, while differences between EM16 and MG2 are larger (Fig. 1). Combining the SWCF and LWCF, the total cloud forcing is generally within a few W m^{-2} for MG2, EM16, and P3, with the largest differences in the Southern Hemisphere midlatitude storm track where total cloud forcing in P3 and EM16 is about 5 W m^{-2} less than MG2 (Fig. 1c). Compared to the CERES observations of SWCF and LWCF, MG2 is closest to the observations in the tropics with biases of up to 10 and -4 W m^{-2} for SWCF and LWCF, respectively. EM16 is somewhat closer to CERES in the midlatitudes with a bias of up to -5 W m^{-2} for SWCF and -3 W m^{-2} for LWCF. However, all simulations have a magnitude of the SWCF and LWCF that is biased high and low, respectively, in the midlatitudes compared to CERES.

An analysis of microphysical quantities helps to explain these differences in cloud radiative forcing among the simulations. Figure 3 shows the total ice water path (IWP) and the cloud droplet water path (LWP). The LWP is similar among all of the simulations. IWP is somewhat lower in EM16 and P3 than MG2 in the midlatitudes but somewhat higher in the tropics. Thus, in the midlatitudes, EM16 and P3 have generally similar cloud radiative forcing despite having lower IWP compared to MG2. On the other hand, in the tropics where the IWP is somewhat larger in EM16 and P3 than MG2,

the cloud forcing is much higher. These results are partly explained by differences in the high cloud fraction (above 400 hPa) among the simulations, which are small globally (within a few %; see Table 1) but larger (higher by 2% and 7% in P3 and EM16, respectively, than MG2) in the tropics (30°S to 30°N). In contrast, high cloud fraction in the extratropics is $\sim 2\%$ smaller in P3 than MG2 and similar between EM16 and MG2.

Differences in the distribution of atmospheric ice are further illustrated by global maps and zonal mean vertical cross sections of ice water content (IWC) from MG2, EM16, and P3 (Fig. 4). Also shown in Fig. 4 are retrievals from CloudSat and MLS. Note that there are limitations in the CloudSat retrievals; low-level clouds (located less than about 1 km above the surface) are not observable owing to surface contamination in the retrieval signal. Furthermore, the IWC retrieval assumes a temperature-dependent phase partitioning in the mixed-phased regime between 0° and -20°C . All three simulations have a global distribution of IWC qualitatively similar to the retrievals. Notable biases compared to the retrieved IWC that are common to all of the simulations are a lower magnitude in the tropics at high altitudes (20 mg m^{-3} in the retrievals compared to 5 mg m^{-3} in the simulations) and a peak IWC in mid-latitudes that occurs at lower altitudes ($\sim 600 \text{ hPa}$ in the retrievals and close to the surface in the simulations). P3 and especially EM16 have IWC closer to the retrievals in the tropical mid- and upper troposphere compared to MG2, while EM16 overestimates IWC in the subtropical regions off the west coast of continents compared to MG2 and P3.

Differences in cloud radiative forcing among the simulations are also partly explained by differences in ice effective radius in addition to the differences in the IWP/IWC, with zonal mean values at cloud top shown in Fig. 5. The cloud ice effective radius is shown in Fig. 5 for MG2, since it has a greater impact on radiative forcing than snow (both are included in the radiative transfer, but the mean effective radius for snow is roughly

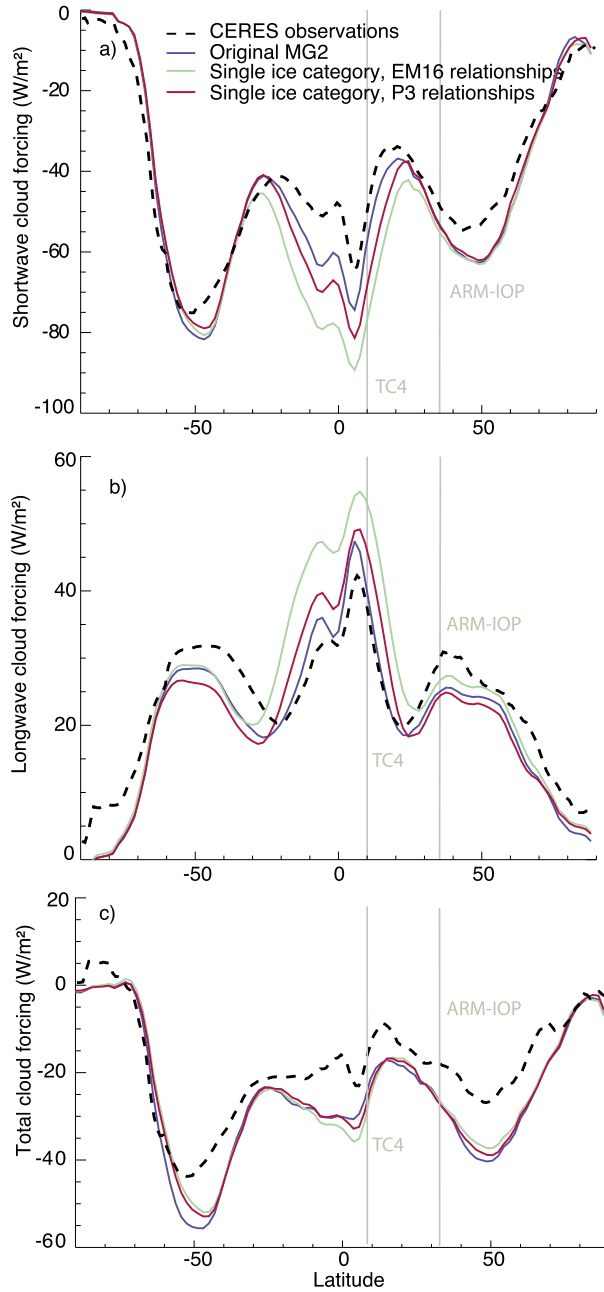


FIG. 1. Zonal mean (a) SWCF, (b) LWCF, and (c) total cloud forcing for MG2 (blue), EM16 (green), and P3 (red). CERES observations are shown by the black dashed lines. Also indicated are locations of the TC4 and ARM-IOP field campaigns (vertical gray lines).

2–3 times that for cloud ice for a given location). The ice effective radius in EM16 and P3 is about one-half the cloud ice effective radius from MG2 in the midlatitudes (including the contribution from snow in MG2 would increase these differences further). This compensates for the smaller IWP in EM16 and P3 so that the LWCF

and SWCF are similar to MG2 in the midlatitudes since both LWCF and SWCF are inversely proportional to effective radius. Note that Erfani and Mitchell (2016) show in their Fig. 13 that in MG2, where ice particles are assumed to be spherical, the effective radius is largely overestimated when the mean diameter is greater than about 100 μm . However, in the tropics the effective radius is only about 3–5 μm smaller in EM16 and P3 than MG2, but the IWP and high cloud fraction are larger as noted above, explaining the larger magnitude of SWCF and LWCF in EM16 and P3 than MG2 there. Differences in cloud-top ice effective radius between P3 and EM16 are small, generally less than 1 μm . Thus, differences in LWCF and SWCF between these simulations are mainly attributable to the differences in IWP and high cloud fraction, rather than effective radius.

The main difference between EM16 and P3 is calculation of the process rates and microphysical properties due to the use of different m - D and A - D relationships. To determine which specific microphysical process or property from the calculations is most responsible for differences between the two simulations (EM16 and P3), we ran several test simulations where one of the processes or properties in the EM16 lookup table was replaced with one from the P3 lookup table (effective radius, mass-/number-weighted fall speed, vapor deposition, and so forth). Most of these tests revealed little difference in cloud radiative forcing using EM16 process/property calculations compared to using process rates or properties swapped from P3 (not shown). However, by using the mass-weighted and number-weighted mean fall speeds from P3 in EM16 and keeping all other process rate and property calculations the same, the LWCF and SWCF are nearly the same as in P3 (Fig. 6). This shows that sedimentation of ice is a key process, responsible for the ~ 4 – 8 W m^{-2} difference in the tropical SWCF and LWCF between EM16 and P3 and broadly consistent with previous studies showing the importance of ice sedimentation on cloud radiative forcing in earlier versions of CAM (Mitchell et al. 2008).

This finding is further supported by an analysis of several individual (nonsedimentation) mass microphysical process rate profiles averaged over the tropics (Fig. 7). There are large differences in process rates between EM16 and MG2 and between P3 and MG2, especially deposition and sublimation of ice and snow, while differences between EM16 and P3 are much smaller, indicating similarity of the process rates in these two simulations. Interestingly, MG2 shows a deep region with net sublimation between 400 and 700 hPa, while there is weak sublimation or net deposition across these levels in EM16 and P3. This difference is directly attributable to the representation of snow in MG2, for

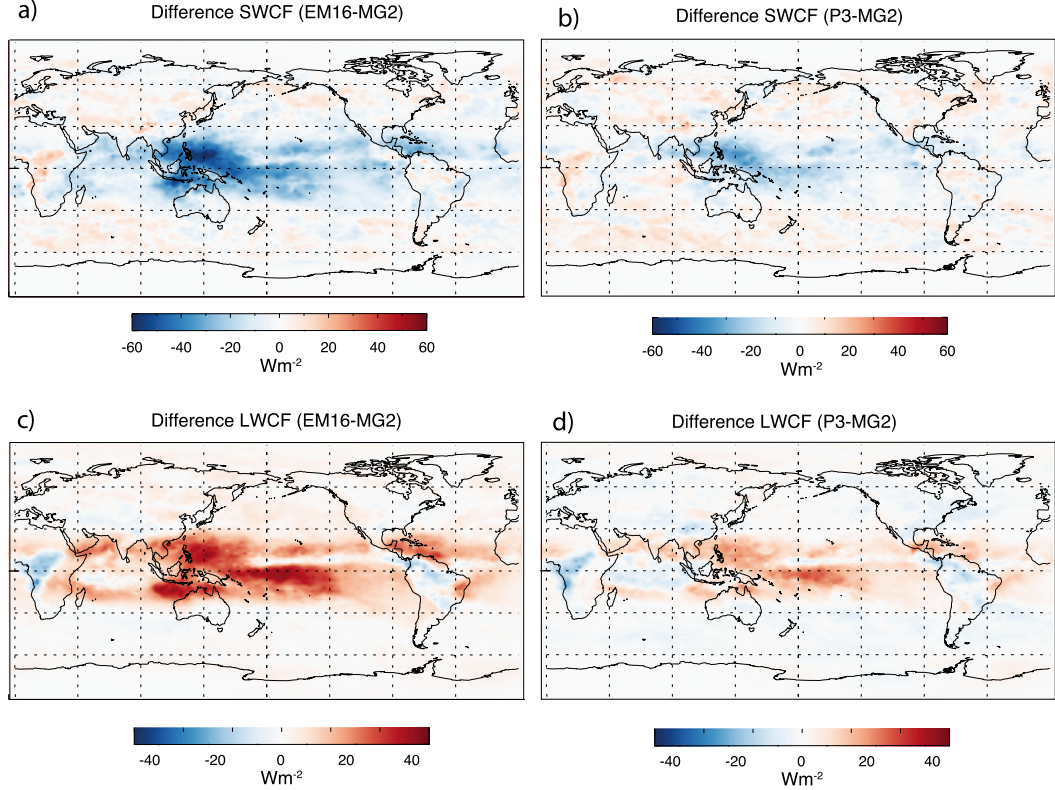


FIG. 2. Differences in zonal mean (a),(b) SWCF and (c),(d) LWCF between MG2 and either (left) EM16 or (right) P3.

which sublimation is allowed but vapor deposition is neglected. In contrast, particles of all sizes can undergo vapor deposition and sublimation in EM16 and P3, improving physical realism and consistency. In addition, there are other significant differences in process rates between MG2 and the other two schemes, and these may relate to the use of spherical ice in MG2. Using a steady-state height-dependent snow growth model, Mitchell (1988) demonstrated how the PSD evolution

was strongly altered by using spherical ice compared to more realistic m - D power laws.

b. Mass-weighted mean terminal fall speed

The mass-weighted mean terminal fall speed of ice V_m is an important property because it impacts sedimentation and was shown in the previous subsection to be critical for explaining differences in cloud radiative forcing among the simulations. Thus, we compare values

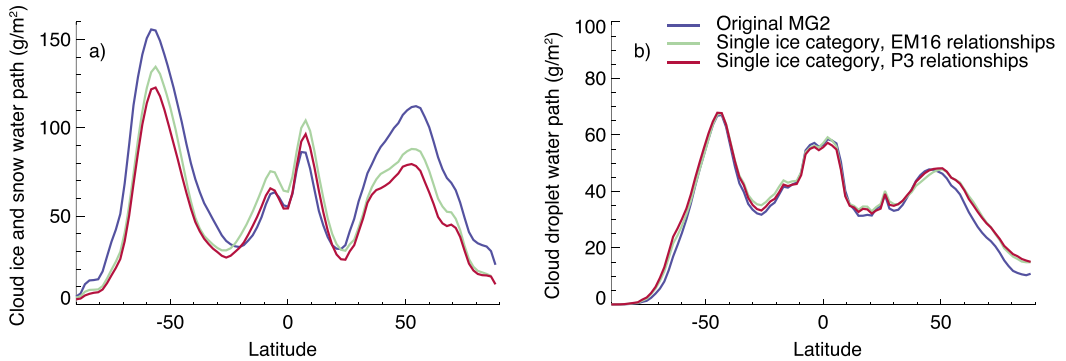


FIG. 3. Zonal mean (a) ice water path (cloud ice + snow for the MG2 simulation) and (b) cloud droplet water path. Colors as in Fig. 1.

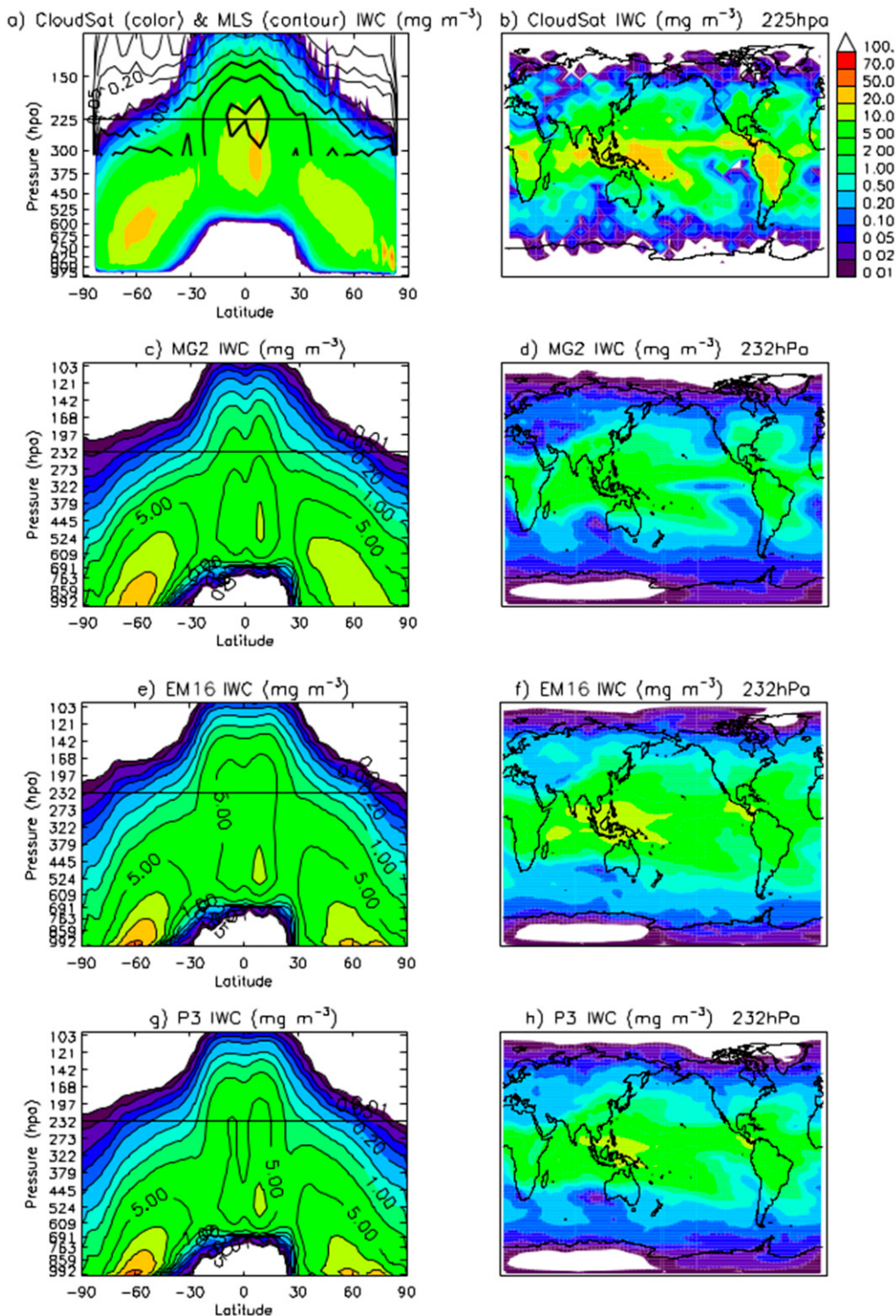


FIG. 4. Zonal mean-pressure plots of ice water content from (a) *CloudSat* (color contour) and Microwave Limb Sounder (black contour lines) retrievals and (c) MG2, (e) EM16, and (g) P3 simulations. Global maps of ice water content (b) at 225 hPa from the *CloudSat* retrieval and (d) at 232 hPa from the MG2, (f) EM16, and (h) P3 simulations. Note that IWC from MG2 includes cloud ice and snow, while in EM16 and P3 it is from the single ice category. Contour intervals are the same as the in the color bars.

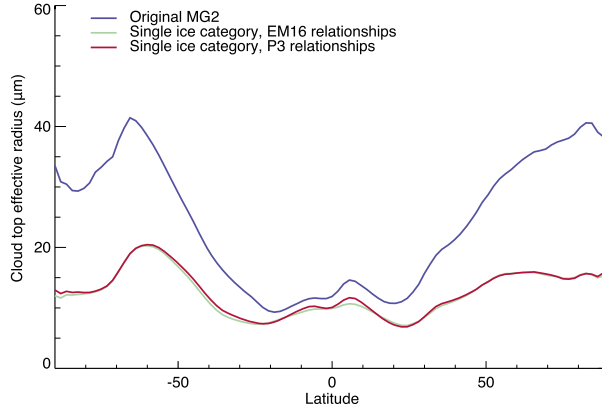


FIG. 5. Zonal mean cloud-top ice effective radius. Colors as in Fig. 1.

of V_m to further explore differences among the simulations. Estimates of V_m from in situ observations were made during the ARM–DOE and TC4 aircraft campaigns. Details of how the V_m are calculated from the observations are given in Eidhammer et al. (2014) and references therein. Calculation of a combined cloud ice and snow mass-weighted terminal fall speed from MG2 is also explained in Eidhammer et al. (2014), while for P3 and EM16, the V_m are calculated following the approach described in section 2c.

Figure 8 shows V_m from the simulations using MG2, EM16, and P3, along with the observed estimates from TC4 and ARM-IOP. The observed clouds in TC4 were dominated by anvil cirrus while the observations from ARM-IOP were primarily of midlatitude frontal clouds. The modeled V_m are a compilation of five years of model data, covering the same region (Fig. 1 in Eidhammer et al. 2014) and the same month as the observations. The V_m from MG2 here are similar to the results shown in Eidhammer et al. (2014, their Fig. 7) with $D_{cs} = 250 \mu\text{m}$, even though they used a different version of the microphysics (MG1.5 instead of MG2; nonetheless, the same power law fall speed-size relationships are used in both schemes). The V_m from MG2 are lower overall compared to observed estimates and have a sharp decrease at colder temperatures. In contrast, the V_m from EM16 and P3 have a weaker increase with temperature, reaching about 1 m s^{-1} at 0°C , more consistent with observations. Overall, P3 has larger V_m than EM16, especially at lower temperatures, which helps to explain why P3 has smaller IWC in the upper troposphere than EM16 (Fig. 4) and smaller IWP (Fig. 3a) due to greater fall speed and hence increased removal by sedimentation. MG2 is able to somewhat better capture the observations showing smaller V_m during ARM-IOP than TC4. Even though TC4 was dominated by anvil cirrus,

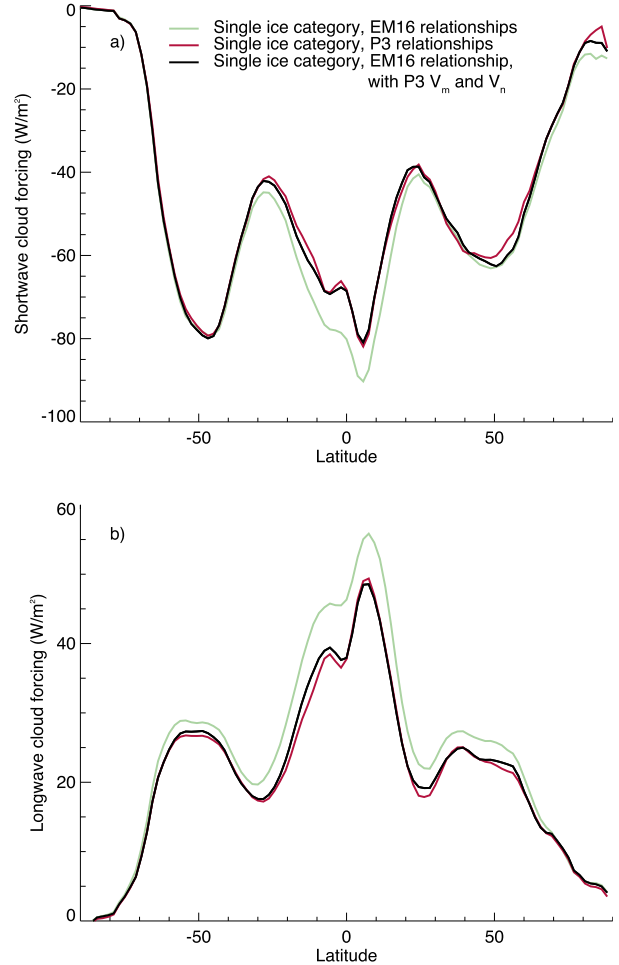


FIG. 6. Zonal mean (a) SWCF and (b) LWCF using EM16 (green), P3 (red), and EM16 with V_m and V_n from P3 (black).

using m – D and A – D parameters derived from measurements in anvil instead of in situ cirrus in EM16 has little impact on V_m (not shown). However, it is worth pointing out that both the in situ and anvil cirrus measurements were made in a continental midlatitude environment contrasting with the tropical maritime environment of TC4, which could explain the limited sensitivity. Furthermore, additional sensitivity tests, using the same values of m – D and A – D parameters over all temperature ranges also had little impact on V_m (not shown).

c. Impact of homogeneous freezing of deliquescent aerosols

In GCMs there are several parameters that must be tuned or adjusted so that the model reasonably represents Earth's climate system, such as top-of-atmosphere radiative balance, global mean temperature, or sea ice distribution (e.g., Mauritsen et al. 2012). With changes

2002-2006 Tropics

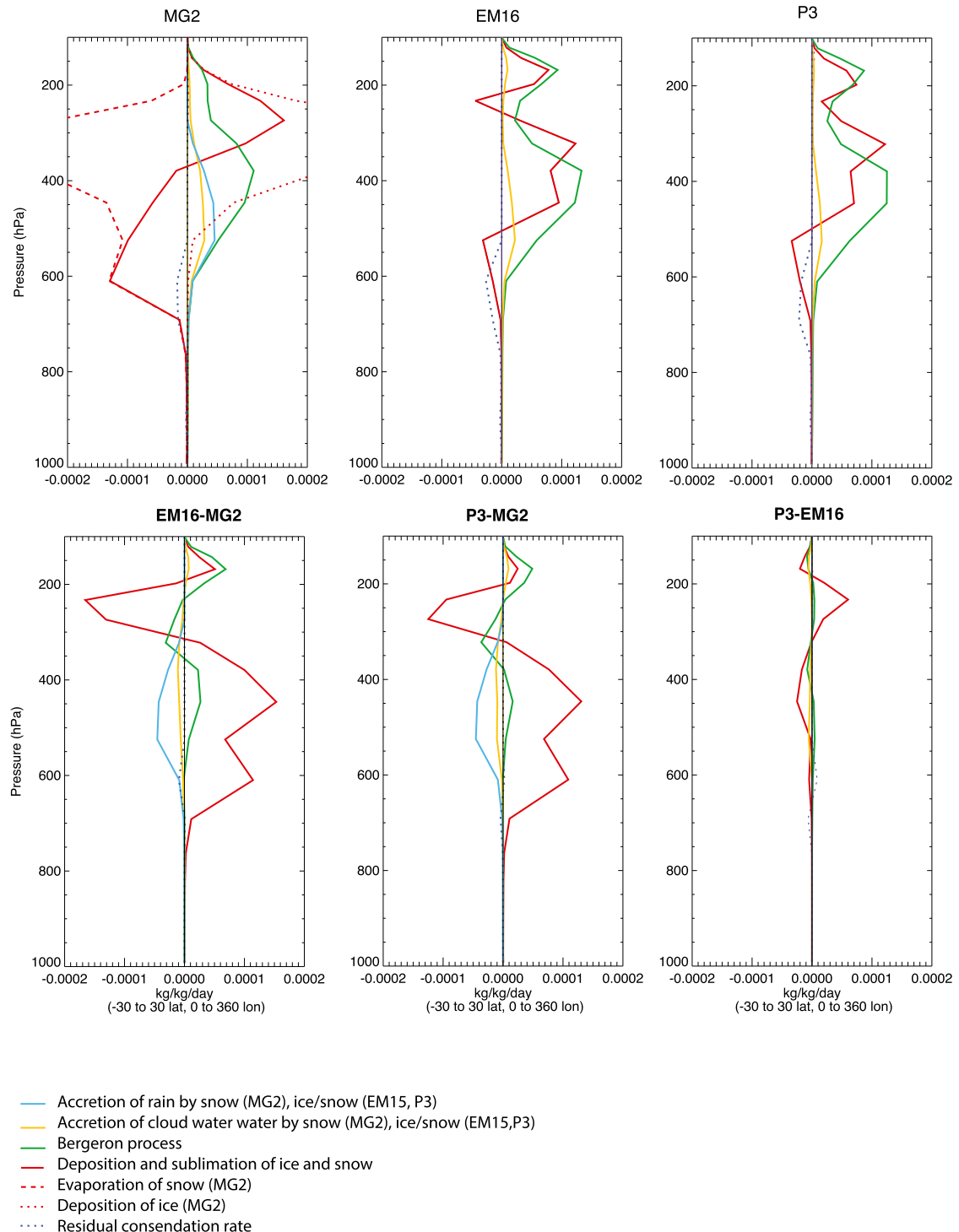


FIG. 7. (top) Vertical profiles of microphysical process rates averaged over the tropics (30°S to 30°N latitude) using (left) MG2, (center) EM16, and (right) P3. (bottom) Process rate differences between the three simulations. Cloud ice and snow processes are combined for MG2 except for sublimation of snow and deposition and sublimation of cloud ice. “Deposition and sublimation of ice” for MG2 is the sum of snow sublimation and cloud ice deposition and sublimation.

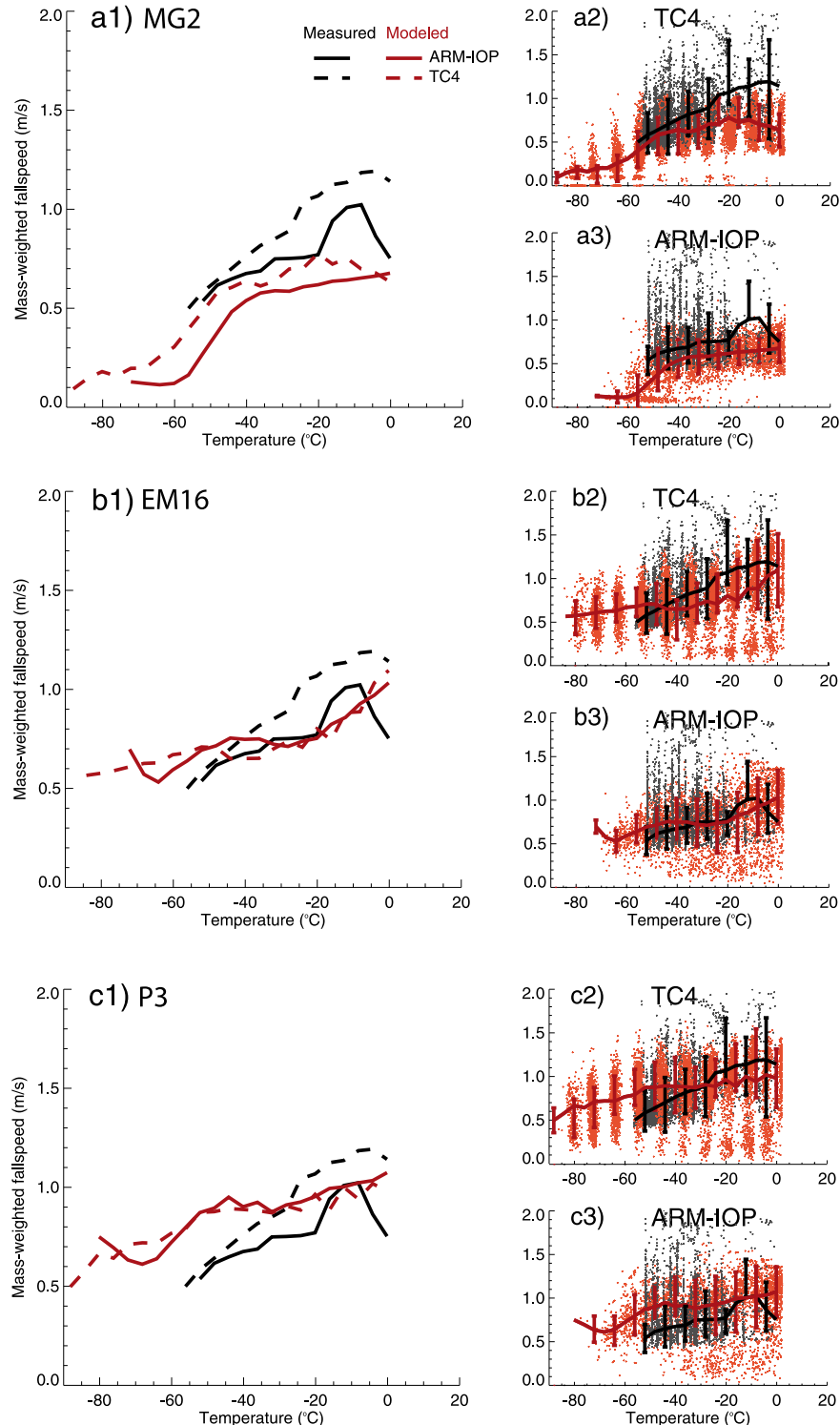


FIG. 8. Modeled and observed mass-weighted terminal fall speeds for TC4 and ARM-IOP as a function of air temperature for (top) MG2, (middle) EM16, and (bottom) P3. (left) Mean values; (right) individual data points and one standard deviation spread (vertical bars).

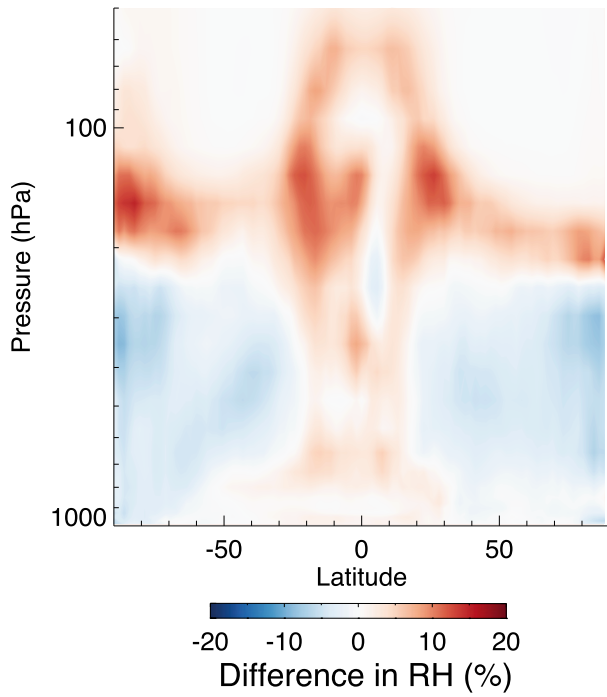


FIG. 9. Differences in zonal mean relative humidity (EM16 – MG2).

to physical parameterizations or other aspects of the model, the previous tuning might cause imbalances in the simulated climate, and therefore retuning is required. Here the top-of-atmosphere radiative imbalance with specified SSTs is 2.5 W m^{-2} for MG2 and $\sim 0.5 \text{ W m}^{-2}$ for EM16 and P3 (Table 1). Typically fixed SST simulations do not have zero energy balance since CAM5 is tuned for zero balance in a preindustrial (1850 boundary conditions) coupled land–atmosphere–ocean–ice simulation.

Greater cloud radiative forcing in the tropics in EM16 relative to MG2 is due to an increase of IWP and cloud fraction as discussed above. As can be seen in Figs. 4c,e, the average zonal mean ice water content is generally lower in EM16 than MG2 at altitudes below 300 hPa but higher at altitudes above 300 hPa. These thin high clouds have a large impact on cloud radiative forcing since they reflect incoming shortwave radiation and are efficient in trapping the longwave outgoing radiation. EM16 also has greater relative humidity ($\sim 15\%$) in the tropics (Fig. 9), which moistens the atmosphere around 200 hPa compared to MG2 enough to increase the homogeneous freezing of deliquescent aerosols and hence ice water content. Thus, we modified parameters that affect the homogeneous freezing of aerosols to explore some possible tunings.

Ice nucleation is described in Gettelman et al. (2010), and they specifically point out that there are several

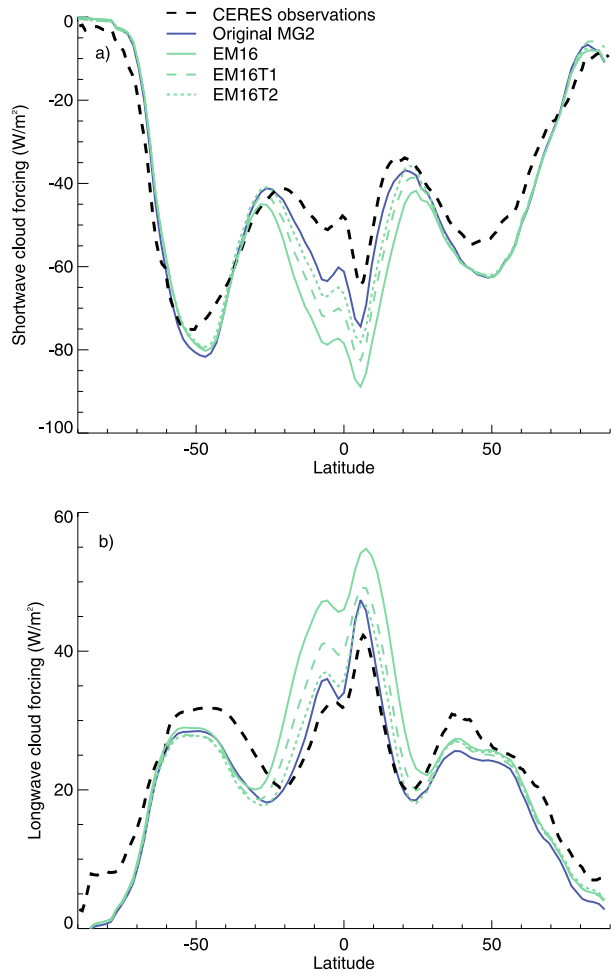


FIG. 10. Zonal mean (a) SWCF and (b) LWCF from observations (black dotted), MG2 (blue), EM16 (green solid), and tests EM16T1 (green dotted) and EM16T2 (green dashed).

uncertainties when parameterizing ice crystal nucleation in a GCM, such as assumptions of subgrid velocity and humidity, ice cloud fraction, and the nucleating ability of aerosols. We tested the effects of reducing the homogeneous freezing of deliquescent aerosols in two different ways to reduce the radiative forcing in the tropics. In the first test (EM16T1), we introduced a temperature-dependent increase in the RH threshold when calculating homogeneous freezing, which allows for a reduction of the homogeneous freezing of deliquescent aerosols and a resulting decrease in cloud radiative forcing (Fig. 10). Second, in the standard CAM5 it is assumed that sulfate aerosols greater than 100 nm (Gettelman et al. 2010) are available for the homogeneous freezing of deliquescent aerosols. This lower size limit was introduced as a tuning for CAM5 to match modeled ice number concentration with observations of ice number concentration in Krämer et al. (2009)

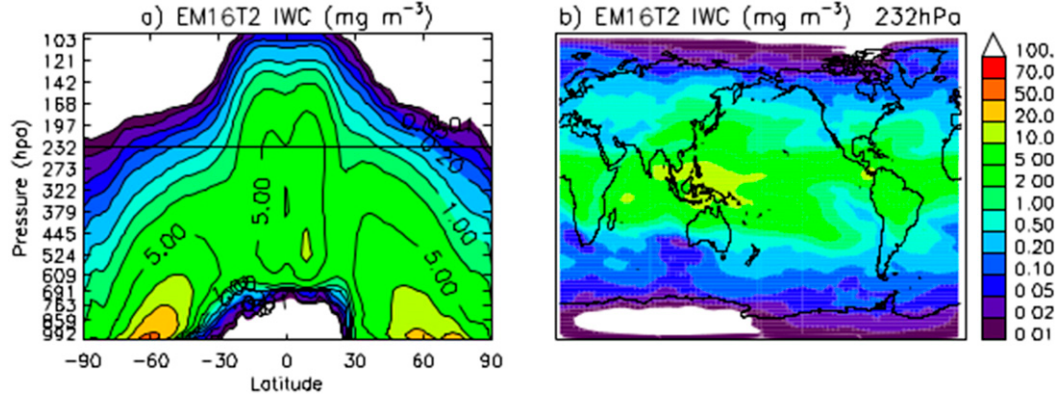


FIG. 11. As in Fig. 4, but with test EM16T2.

(X. Liu 2016, personal communication). In the second test (EM16T2), we modified the RH threshold for calculating homogeneous freezing and also increased this limit to 200 nm, which decreases the number of sulfate aerosols that can activate at a given temperature, to further reduce homogeneous freezing. This produces an overall decrease in the IWC compared to EM16, although it is still greater than in MG2 and more similar to CloudSat and MLS in the tropical troposphere (cf. Fig. 11 and Fig. 4). This decreases the magnitude of the cloud radiative forcing in the tropics compared to EM16 (Fig. 10), with EM16T2 similar to MG2 (Fig. 12). However, the mean particle size is also increased, resulting in larger V_m at temperatures less than -40°C and a larger bias than EM16 relative to the observed estimates, mainly for TC4 (cf. Fig. 13 and Fig. 8b). We emphasize that this should be viewed as an initial exploratory set of tuning experiments and anticipate that more detailed tuning will help to address these issues. Such an effort is beyond the scope of this paper but is planned for future work.

5. Summary and conclusions

This paper describes conceptual improvements to the representation of ice microphysics in CAM5. The existing MG2 microphysics scheme (Morrison and Gettelman 2008; Gettelman and Morrison 2015) separates ice into two categories representing small ice (cloud ice) and larger ice (snow). All ice particles are assumed to be spherical, with different bulk densities and fall speed-size relationships employed for cloud ice and snow. Conversion of mass and number mixing ratios between the cloud ice and snow categories occurs through autoconversion and accretion processes, the former determined by a threshold size parameter D_{cs} that is uncertain and poorly constrained by theory or

observations. Simulated climate, including cloud radiative forcing, is sensitive to specification of D_{cs} (Zhang et al. 2013; Eidhammer et al. 2014). Another shortcoming of MG2, similar to most bulk schemes, is that particle mass, projected area, and terminal fall speed are not treated consistently for all parameters and processes.

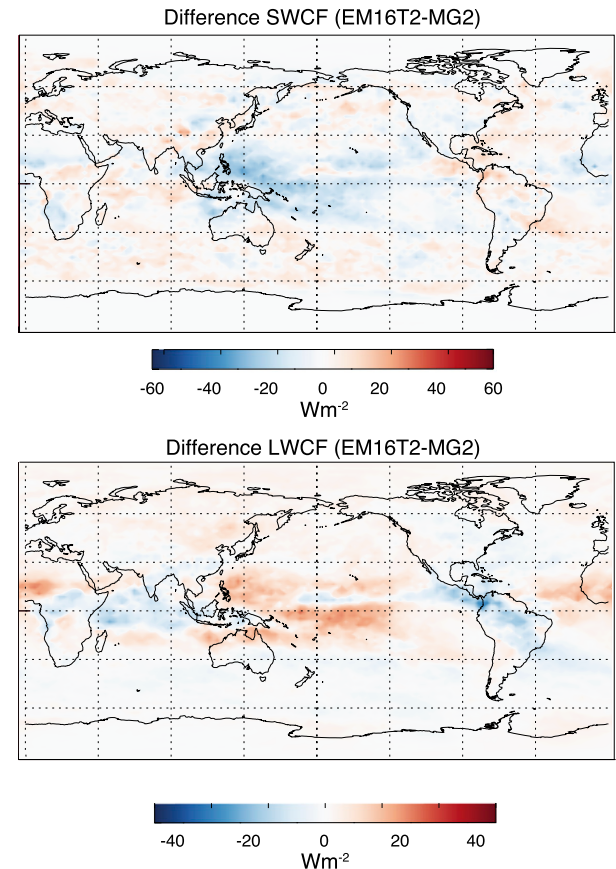


FIG. 12. As in Fig. 2, but with test EM16T2.

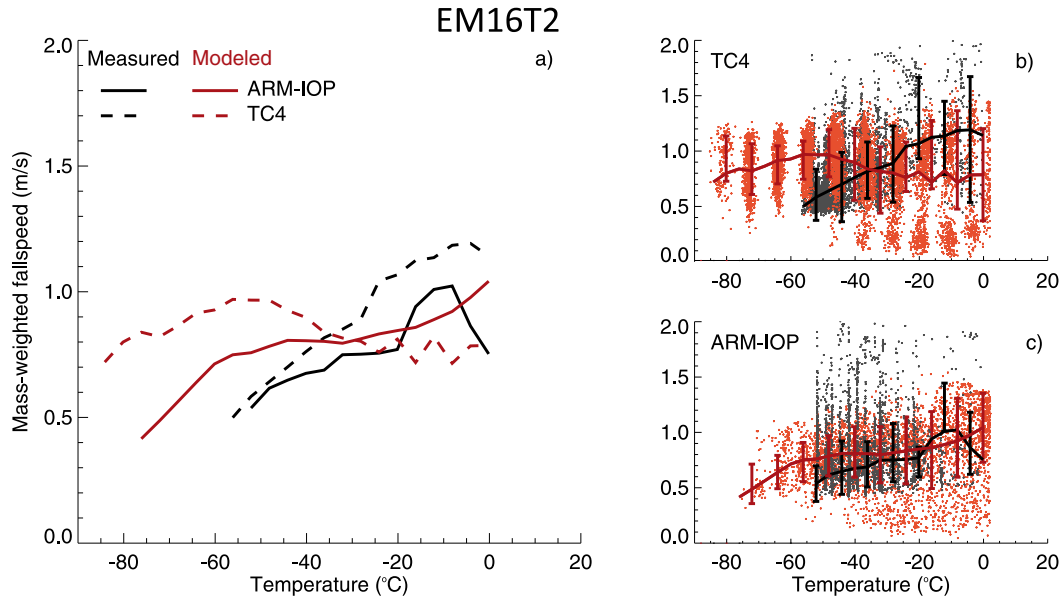


FIG. 13. As in Fig. 8, but with test EM16T2.

The modified scheme uses a single ice category so that conversion between cloud ice and snow and specification of D_{cs} are no longer needed. To improve self-consistency, all relevant microphysical processes and parameters are formulated in terms of particle mass-size (m - D) and projected area-size (A - D) relationships that vary with particle size. This allows the scheme to smoothly represent the transition between higher density small ice particles and lower density large particles, in the spirit of recent bulk approaches that do not separate ice into different predefined categories and smoothly represent m - D and A - D relationships (Morrison and Grabowski 2008; Harrington et al. 2013a,b; Morrison and Milbrandt 2015). Note that this approach also represents a simplification of the microphysics compared to MG2, since there are six instead of eight total prognostic microphysical variables. Two methods for specifying the m - D and A - D relationships were implemented and tested. The first (EM16) was based on cirrus observations during the SPARTICUS field campaign (Erfani and Mitchell 2016). The second method (P3) was based on the approach of Morrison and Milbrandt (2015).

Global simulations using the modified microphysics were performed and compared with those using the original MG2 microphysics. Total cloud radiative forcing (SWCF + LWCF) was similar among all of the simulations, with zonal mean differences less than 5 W m^{-2} for all latitudes. However, EM16 produced a larger magnitude of the annual and zonal mean SWCF and LWCF in the tropics compared to MG2 by up to

about 14 and 8 W m^{-2} , respectively, with smaller differences between P3 and MG2. In the midlatitudes, the ice effective radius in EM16 and P3 was about one-half the cloud ice effective radius from MG2 in the midlatitudes, compensating for smaller IWP in EM16 and P3 so that the LWCF and SWCF were similar to MG2. On the other hand, ice effective radius was only a few μm smaller in EM16 and P3 than MG2 in the tropics, while IWP and high cloud fraction were higher, explaining why the magnitude of SWCF and LWCF were larger in P3 and especially EM16 compared to MG2. Ice water content (IWC) in the upper tropical troposphere in EM16 was larger than in P3 and especially MG2 and closer to CloudSat and MLS retrievals, although EM16 tended to overestimate IWC in subtropical regions off the west coasts of continents.

Additional tests showed that sedimentation of ice is responsible for the ~ 4 – 8 W m^{-2} difference in the tropical SWCF and LWCF between EM16 and P3. EM16 and P3 had mass-weighted mean fall speeds for ice as a function of temperature overall closer to aircraft observations during the ARM-IOP and TC4 field experiments than MG2, although neither EM16 nor P3 were able to capture the observed tendency for larger mean fall speeds during TC4 compared to ARM-IOP. P3 gave somewhat larger mean fall speeds than EM16, consistent with greater removal of mass through sedimentation and reduced IWP compared to EM16.

While the main goal of this study was to demonstrate proof of concept in simulating climate using the new

approach, some tuning using EM16 was explored by performing additional simulations with homogeneous freezing of aerosols decreased in order to reduce the magnitude of the tropical SWCF and LWCF. This was done by modifying the subgrid-scale RH dependence and increasing the threshold size of sulfate aerosols available to freeze, reducing IWP in the tropics so that LWCF and SWCF were similar to MG2. While these tests indicate the ability of the new scheme to produce a simulated climate comparable to that from MG2, they also highlight sensitivity of the radiative forcing to uncertain ice nucleation parameters (Gettelman et al. 2012). Detailed tuning of the modified scheme was beyond the scope of this work, but we anticipate further improvements in simulated climate may be possible with additional tuning. For example, there is now an option in CAM5 that allows for including preexisting ice when calculating homogeneous freezing, which has shown to reduce the number of ice crystals in cirrus clouds (Shi et al. 2015). It is also emphasized that more detailed testing is needed in the context of other key aspects of climate, such as modes of tropical variability and climate sensitivity.

This study has proposed a new approach for representing ice microphysics in a GCM, and demonstrated its feasibility using AMIP-type global climate simulations. Results showed that it can produce a comparable climate to MG2 while improving the conceptual basis and self-consistency of ice particle properties and parameters. This study explored two different methods for specifying the m - D and A - D relationships, but the approach is flexible and could be modified to use any set of relationships. These relationships were specified from SPARTICUS observations in the current implementation for EM16 but should be extended to include measurements taken across the globe as they become available.

Acknowledgments. This work was supported by the U.S. DOE ASR DE-SC0005336, sub-awarded through NASA NNX12AH90G. Collaborative work regarding the Erfani–Mitchell parameterization of ice particle mass and projected area was supported by the U.S. DOE ASR DE-0008871. Comments on an earlier version of the manuscript by P. Bogenschutz are appreciated. We also thank A. Bansemer and A. Heymsfield for sharing the observational fall speed data from TC4 and ARM-IOP. High performance computing support from Yellowstone was provided by NCAR’s Computational and Information Systems Laboratory, sponsored by NSF. The National Center for Atmospheric Research is sponsored by the U.S. National Science Foundation (NSF).

REFERENCES

- Brown, P. R. A., and P. N. Francis, 1995: Improved measurements of the ice water content in cirrus using a total water probe. *J. Atmos. Oceanic Technol.*, **12**, 410–414, doi:[10.1175/1520-0426\(1995\)012<0410:IMOTIW>2.0.CO;2](https://doi.org/10.1175/1520-0426(1995)012<0410:IMOTIW>2.0.CO;2).
- Dong, X., P. Minnis, G. G. Mace, W. L. Smith, M. Poellot, R. T. Marchand, and A. D. Rapp, 2002: Comparison of stratus cloud properties deduced from surface, GOES, and aircraft data during the March 2000 ARM Cloud IOP. *J. Atmos. Sci.*, **59**, 3265–3284, doi:[10.1175/1520-0469\(2002\)059<3265:COSCPD>2.0.CO;2](https://doi.org/10.1175/1520-0469(2002)059<3265:COSCPD>2.0.CO;2).
- Eidhammer, T., H. Morrison, A. Bansemer, A. Gettelman, and A. J. Heymsfield, 2014: Comparison of ice cloud properties simulated by the Community Atmosphere Model (CAM5) with in-situ observations. *Atmos. Chem. Phys.*, **14**, 10103–10118, doi:[10.5194/acp-14-10103-2014](https://doi.org/10.5194/acp-14-10103-2014).
- Erfani, E., and D. L. Mitchell, 2016: Developing and bounding ice particle mass- and area-dimension expressions for use in atmospheric models and remote sensing. *Atmos. Chem. Phys.*, **16**, 4379–4400, doi:[10.5194/acp-16-4379-2016](https://doi.org/10.5194/acp-16-4379-2016).
- Fowler, L. D., D. A. Randall, and S. A. Rutledge, 1996: Liquid and ice cloud microphysics in the CSU general circulation model. Part I: Model description and simulated microphysical processes. *J. Climate*, **9**, 489–529, doi:[10.1175/1520-0442\(1996\)009<0489:LAICMI>2.0.CO;2](https://doi.org/10.1175/1520-0442(1996)009<0489:LAICMI>2.0.CO;2).
- Gettelman, A., and H. Morrison, 2015: Advanced two-moment bulk microphysics for global models. Part I: Off-line tests and comparison with other schemes. *J. Climate*, **28**, 1268–1287, doi:[10.1175/JCLI-D-14-00102.1](https://doi.org/10.1175/JCLI-D-14-00102.1).
- , and Coauthors, 2010: Global simulations of ice nucleation and ice supersaturation with an improved cloud scheme in the Community Atmosphere Model. *J. Geophys. Res.*, **115**, D18216, doi:[10.1029/2009JD013797](https://doi.org/10.1029/2009JD013797).
- , X. Liu, D. Barahona, U. Lohmann, and C.-C. Chen, 2012: Climate impacts of ice nucleation. *J. Geophys. Res.*, **117**, D20201, doi:[10.1029/2012JD017950](https://doi.org/10.1029/2012JD017950).
- , H. Morrison, S. Santos, P. Bogenschutz, and P. M. Caldwell, 2015: Advanced two-moment bulk microphysics for global models. Part II: Global model solutions and aerosol–cloud interactions. *J. Climate*, **28**, 1288–1307, doi:[10.1175/JCLI-D-14-00103.1](https://doi.org/10.1175/JCLI-D-14-00103.1).
- Ghan, S. J., and R. C. Easter, 1992: Computationally efficient approximations to stratiform cloud microphysics parameterization. *Mon. Wea. Rev.*, **120**, 1572–1582, doi:[10.1175/1520-0493\(1992\)120<1572:CEATSC>2.0.CO;2](https://doi.org/10.1175/1520-0493(1992)120<1572:CEATSC>2.0.CO;2).
- , L. R. Leung, and R. C. Easter, 1997: Prediction of cloud droplet number in a general circulation model. *J. Geophys. Res.*, **102**, 21 777–21 794, doi:[10.1029/97JD01810](https://doi.org/10.1029/97JD01810).
- Hall, W. D., and H. R. Pruppacher, 1976: The survival of ice particles falling from cirrus clouds in subsaturated air. *J. Atmos. Sci.*, **33**, 1995–2006, doi:[10.1175/1520-0469\(1976\)033<1995:TSOIPF>2.0.CO;2](https://doi.org/10.1175/1520-0469(1976)033<1995:TSOIPF>2.0.CO;2).
- Harrington, J. Y., K. Sulia, and H. Morrison, 2013a: A method for adaptive habit prediction in bulk microphysical models. Part I: Theoretical development. *J. Atmos. Sci.*, **70**, 349–364, doi:[10.1175/JAS-D-12-040.1](https://doi.org/10.1175/JAS-D-12-040.1).
- , —, and —, 2013b: A method for adaptive habit prediction in bulk microphysical models. Part II: Parcel model corroboration. *J. Atmos. Sci.*, **70**, 365–376, doi:[10.1175/JAS-D-12-0152.1](https://doi.org/10.1175/JAS-D-12-0152.1).
- Hashino, T., and G. J. Tripoli, 2007: The Spectral Ice Habit Prediction System (SHIPS). Part I: Model description and simulation of the

- vapor deposition process. *J. Atmos. Sci.*, **64**, 2210–2237, doi:[10.1175/JAS3963.1](https://doi.org/10.1175/JAS3963.1).
- Heymsfield, A. J., 1982: A comparative study of the rates of development of potential graupel and hail embryos in High Plains storms. *J. Atmos. Sci.*, **39**, 2867–2897, doi:[10.1175/1520-0469\(1982\)039<2867:ACSOTR>2.0.CO;2](https://doi.org/10.1175/1520-0469(1982)039<2867:ACSOTR>2.0.CO;2).
- , 2003: Properties of tropical and midlatitude ice cloud particle ensembles. Part II: Applications for mesoscale and climate models. *J. Atmos. Sci.*, **60**, 2592–2611, doi:[10.1175/1520-0469\(2003\)060<2592:POTAMI>2.0.CO;2](https://doi.org/10.1175/1520-0469(2003)060<2592:POTAMI>2.0.CO;2).
- , and C. D. Westbrook, 2010: Advances in the estimation of ice particle fall speeds using laboratory and field measurements. *J. Atmos. Sci.*, **67**, 2469–2482, doi:[10.1175/2010JAS3379.1](https://doi.org/10.1175/2010JAS3379.1).
- Hong, S.-Y., J. Dudhia, and S.-H. Chen, 2004: A revised approach to ice microphysical processes for the bulk parameterization of clouds and precipitation. *Mon. Wea. Rev.*, **132**, 103–120, doi:[10.1175/1520-0493\(2004\)132<0103:ARATIM>2.0.CO;2](https://doi.org/10.1175/1520-0493(2004)132<0103:ARATIM>2.0.CO;2).
- Krämer, M., and Coauthors, 2009: Ice supersaturations and cirrus cloud crystal numbers. *Atmos. Chem. Phys.*, **9**, 3505–3522, doi:[10.5194/acp-9-3505-2009](https://doi.org/10.5194/acp-9-3505-2009).
- Lawson, R. P., and A. Gettelman, 2014: Impact of Antarctic mixed-phase clouds on climate. *Proc. Natl. Acad. Sci. USA*, **111**, 18 156–18 161, doi:[10.1073/pnas.1418197111](https://doi.org/10.1073/pnas.1418197111).
- Liu, X., and J. E. Penner, 2005: Ice nucleation parameterization for global models. *Meteor. Z.*, **14**, 499–514, doi:[10.1127/0941-2948/2005/0059](https://doi.org/10.1127/0941-2948/2005/0059).
- , —, S. J. Ghan, and M. Wang, 2007: Inclusion of ice microphysics in the NCAR Community Atmosphere Model version 3 (CAM3). *J. Climate*, **20**, 4526–4547, doi:[10.1175/JCLI4264.1](https://doi.org/10.1175/JCLI4264.1).
- Lohmann, U., and E. Roeckner, 1996: Design and performance of a new cloud microphysics scheme developed for the ECHAM4 general circulation model. *Climate Dyn.*, **12**, 557–572, doi:[10.1007/BF00207939](https://doi.org/10.1007/BF00207939).
- , J. Feichter, C. C. Chuang, and J. Penner, 1999: Prediction of the number of cloud droplets in the ECHAM GCM. *J. Geophys. Res.*, **104**, 9169–9198, doi:[10.1029/1999JD900046](https://doi.org/10.1029/1999JD900046).
- Lopez, P., 2002: Implementation and validation of a new prognostic large-scale cloud and precipitation scheme for climate and data-assimilation purposes. *Quart. J. Roy. Meteor. Soc.*, **128**, 229–257, doi:[10.1256/00359000260498879](https://doi.org/10.1256/00359000260498879).
- Mauritsen, T., and Coauthors, 2012: Tuning the climate of a global model. *J. Adv. Model. Earth Syst.*, **4**, M00A01, doi:[10.1029/2012MS000154](https://doi.org/10.1029/2012MS000154).
- Meyers, M. P., P. J. DeMott, and W. R. Cotton, 1992: New primary ice nucleation parameterizations in an explicit cloud model. *J. Appl. Meteor.*, **31**, 708–721, doi:[10.1175/1520-0450\(1992\)031<0708:NPINPI>2.0.CO;2](https://doi.org/10.1175/1520-0450(1992)031<0708:NPINPI>2.0.CO;2).
- Milbrandt, J. A., and M. K. Yau, 2005: A multimoment bulk microphysics parameterization. Part I: Analysis of the role of the spectral shape parameter. *J. Atmos. Sci.*, **62**, 3051–3064, doi:[10.1175/JAS3534.1](https://doi.org/10.1175/JAS3534.1).
- , A. Glazer, and D. Jacob, 2012: Predicting the snow-to-liquid ratio of surface precipitation using a bulk microphysics scheme. *Mon. Wea. Rev.*, **140**, 2461–2476, doi:[10.1175/MWR-D-11-00286.1](https://doi.org/10.1175/MWR-D-11-00286.1).
- Ming, Y., V. Ramaswamy, L. J. Donner, V. T. J. Phillips, S. A. Klein, P. A. Ginoux, and L. W. Horowitz, 2007: Modeling the interactions between aerosols and liquid water clouds with a self-consistent cloud scheme in a general circulation model. *J. Atmos. Sci.*, **64**, 1189–1209, doi:[10.1175/JAS3874.1](https://doi.org/10.1175/JAS3874.1).
- Mitchell, D. L., 1988: Evolution of snow-size spectra in cyclonic storms. Part I: Snow growth by vapor deposition and aggregation. *J. Atmos. Sci.*, **45**, 3431–3451, doi:[10.1175/1520-0469\(1988\)045<3431:EOSSSI>2.0.CO;2](https://doi.org/10.1175/1520-0469(1988)045<3431:EOSSSI>2.0.CO;2).
- , and A. J. Heymsfield, 2005: Refinements in the treatment of ice particle terminal velocities, highlighting aggregates. *J. Atmos. Sci.*, **62**, 1637–1644, doi:[10.1175/JAS3413.1](https://doi.org/10.1175/JAS3413.1).
- , A. Macke, and Y. Liu, 1996: Modeling cirrus clouds. Part II: Treatment of radiative properties. *J. Atmos. Sci.*, **53**, 2967–2988, doi:[10.1175/1520-0469\(1996\)053<2967:MCCPIT>2.0.CO;2](https://doi.org/10.1175/1520-0469(1996)053<2967:MCCPIT>2.0.CO;2).
- , P. Rasch, D. Ivanova, G. McFarquhar, and T. Nousiainen, 2008: The impact of small ice crystal assumptions on sedimentation rates and GCM simulations. *Geophys. Res. Lett.*, **35**, L09806, doi:[10.1029/2008GL033552](https://doi.org/10.1029/2008GL033552).
- , S. Mishra, and R. P. Lawson, 2011: Representing the ice fall speed in climate models: Results from Tropical Composition, Cloud and Climate Coupling (TC4) and the Indirect and Semi-Direct Aerosol Campaign (ISDAC). *J. Geophys. Res.*, **116**, D00T03, doi:[10.1029/2010JD015433](https://doi.org/10.1029/2010JD015433).
- Morrison, H., and A. Gettelman, 2008: A new two-moment bulk stratiform cloud microphysics scheme in the NCAR Community Atmosphere Model (CAM3). Part I: Description and numerical tests. *J. Climate*, **21**, 3642–3659, doi:[10.1175/2008JCLI2105.1](https://doi.org/10.1175/2008JCLI2105.1).
- , and W. W. Grabowski, 2008: A novel approach for representing ice microphysics in models: Description and tests using a kinematic framework. *J. Atmos. Sci.*, **65**, 1528–1548, doi:[10.1175/2007JAS2491.1](https://doi.org/10.1175/2007JAS2491.1).
- , and J. A. Milbrandt, 2015: Parameterization of cloud microphysics based on the prediction of bulk ice particle properties. Part I: Scheme description and idealized tests. *J. Atmos. Sci.*, **72**, 287–311, doi:[10.1175/JAS-D-14-0065.1](https://doi.org/10.1175/JAS-D-14-0065.1).
- , G. Thompson, and V. Tatarskii, 2009: Impact of cloud microphysics on the development of trailing stratiform precipitation in a simulated squall line: Comparison of one- and two-moment schemes. *Mon. Wea. Rev.*, **137**, 991–1007, doi:[10.1175/2008MWR2556.1](https://doi.org/10.1175/2008MWR2556.1).
- Neale, R. B., and Coauthors, 2012: Description of the NCAR Community Atmosphere Model (CAM 5.0). NCAR Tech. Note NCAR/TN-486+STR, 289 pp.
- Posselt, R., and U. Lohmann, 2008: Introduction of prognostic rain in ECHAM5: Design and single column model simulations. *Atmos. Chem. Phys.*, **8**, 2949–2963, doi:[10.5194/acp-8-2949-2008](https://doi.org/10.5194/acp-8-2949-2008).
- Pruppacher, H. R., and J. D. Klett, 1997: *Microphysics of Clouds and Precipitation: Second Revised and Enlarged Edition with an Introduction to Cloud Chemistry and Cloud Electricity*. Kluwer Academic Publishers, 954 pp.
- Rasch, P. J., and J. E. Kristjansson, 1998: A comparison of the CCM3 model climate using diagnosed and predicted condensate parameterizations. *J. Climate*, **11**, 1587–1614, doi:[10.1175/1520-0442\(1998\)011<1587:ACOTCM>2.0.CO;2](https://doi.org/10.1175/1520-0442(1998)011<1587:ACOTCM>2.0.CO;2).
- Rotstayn, L. D., B. F. Ryan, and J. J. Katzfey, 2000: A scheme for calculation of the liquid fraction in mixed-phase stratiform clouds in large-scale models. *Mon. Wea. Rev.*, **128**, 1070–1088, doi:[10.1175/1520-0493\(2000\)128<1070:ASFCOT>2.0.CO;2](https://doi.org/10.1175/1520-0493(2000)128<1070:ASFCOT>2.0.CO;2).
- Shi, X., X. Liu, and K. Zhang, 2015: Effects of pre-existing ice crystals on cirrus clouds and comparison between different ice nucleation parameterizations with the Community Atmosphere Model (CAM5). *Atmos. Chem. Phys.*, **15**, 1503–1520, doi:[10.5194/acp-15-1503-2015](https://doi.org/10.5194/acp-15-1503-2015).
- Sulia, K., and J. Y. Harrington, 2011: Ice aspect ratio influences on mixed-phase clouds: Impacts of phase partitioning in parcel models. *J. Geophys. Res.*, **116**, D21309, doi:[10.1029/2011JD016298](https://doi.org/10.1029/2011JD016298).
- Thompson, G., R. M. Rasmussen, and K. Manning, 2004: Explicit forecasts of winter precipitation using an improved bulk

- microphysics scheme. Part I: Description and sensitivity analysis. *Mon. Wea. Rev.*, **132**, 519–542, doi:[10.1175/1520-0493\(2004\)132<0519:EFOWPU>2.0.CO;2](https://doi.org/10.1175/1520-0493(2004)132<0519:EFOWPU>2.0.CO;2).
- , P. R. Field, R. M. Rasmussen, and W. D. Hall, 2008: Explicit forecasts of winter precipitation using an improved bulk microphysics scheme. Part II: Implementation of a new snow parameterization. *Mon. Wea. Rev.*, **136**, 5095–5115, doi:[10.1175/2008MWR2387.1](https://doi.org/10.1175/2008MWR2387.1).
- Toon, O. B., and Coauthors, 2010: Planning, implementation, and first results of the Tropical Composition, Cloud and Climate Coupling Experiment (TC4). *J. Geophys. Res.*, **115**, D00J04, doi:[10.1029/2009JD013073](https://doi.org/10.1029/2009JD013073).
- Waliser, D. E., and Coauthors, 2009: Cloud ice: A climate model challenge with signs and expectations of progress. *J. Geophys. Res.*, **114**, D00A21, doi:[10.1029/2008JD010015](https://doi.org/10.1029/2008JD010015).
- Walters, D. N., and Coauthors, 2014: The Met Office Unified Model Global Atmosphere 4.0 and JULES Global Land 4.0 configurations. *Geosci. Model Dev.*, **7**, 361–386, doi:[10.5194/gmd-7-361-2014](https://doi.org/10.5194/gmd-7-361-2014).
- Wielicki, B. A., B. R. Barkstrom, E. F. Harrison, R. B. Lee III, G. L. Smith, and J. E. Cooper, 1996: Clouds and the Earth's Radiant Energy System (CERES): An Earth observing system experiment. *Bull. Amer. Meteor. Soc.*, **77**, 853–868, doi:[10.1175/1520-0477\(1996\)077<0853:CATERE>2.0.CO;2](https://doi.org/10.1175/1520-0477(1996)077<0853:CATERE>2.0.CO;2).
- Wilson, D. R., and S. P. Ballard, 1999: A microphysically based precipitation scheme for the UK Meteorological Office Unified Model. *Quart. J. Roy. Meteor. Soc.*, **125**, 1607–1636, doi:[10.1002/qj.49712555707](https://doi.org/10.1002/qj.49712555707).
- Wu, D., and Coauthors, 2009: Comparisons of global cloud ice from MLS, CloudSat, and correlative data sets. *J. Geophys. Res.*, **114**, D00A24, doi:[10.1029/2008JD009946](https://doi.org/10.1029/2008JD009946).
- Zhang, K., X. Liu, M. Wang, J. M. Comstock, D. L. Mitchell, S. Mishra, and G. G. Mace, 2013: Evaluating and constraining ice cloud parameterizations in CAM5 using aircraft measurements from the SPARTICUS campaign. *Atmos. Chem. Phys.*, **13**, 4963–4982, doi:[10.5194/acp-13-4963-2013](https://doi.org/10.5194/acp-13-4963-2013).